Dynamic Fracture Analysis Using an Uncoupled Arbitrary Lagrangian Eulerian Finite Element Formulation

A.R. Shahani[*], M.R. Amini

Department of Applied Mechanics, Faculty of Mechanical Engineering, K.N. Toosi University of Technology, Pardis Street, Mollasadra Avenue, Vanak Square, P.O. Box 19395-1999, Tehran, Iran

ABSTRACT

This paper deals with the implementation of an efficient Arbitrary Lagrangian Eulerian (ALE) formulation for the three dimensional finite element modeling of mode *I* self-similar dynamic fracture process. Contrary to the remeshing technique, the presented algorithm can continuously advance the crack with the one mesh topology. The uncoupled approach is employed to treat the equations. So, each time step is split into two phases: an updated Lagrangian phase followed by an Eulerian phase. The implicit time integration method is applied for solving the transient problem in Lagrangian phase with no convective effects. A mesh motion scheme, in which the related equations need not to be solved at every time step, is proposed in Eulerian phase. The critical dynamic stress intensity factor criterion is used to determine the crack velocity. The variation of dynamic stress intensity factor along the crack front is also studied based on the interaction integral method. The proposed algorithm is applied to investigate the dynamic crack propagation in the DCB specimen subjected to fixed displacement. The predicted results are compared with the experimental study cited in the literature and a good agreement is shown. The proposed algorithm leads to the accurate and efficient analysis of dynamic crack propagation process.

© 2011 IAU, Arak Branch. All rights reserved.

Keywords: Three dimensional ALE finite element formulation; Mesh motion; Dynamic fracture; Crack velocity; Implicit dynamic analysis

1 INTRODUCTION

EXACT analytical solutions for the dynamic fracture problem are rarely available because of technical difficulties in solving equations of motion, particularly for complex geometries. So, the analytical solutions may only be established for the simple cases. Recently, an analytical modeling of dynamic fracture in a DCB specimen is accomplished by means of the Timoshenko beam theory through the quasi-static treatment of unstable crack propagation by Shahani and Amini [1]. They obtained the closed forms for the stress intensity factor, strain energy, kinetic energy and crack velocity in DCB specimen, which are functions of the model dimensions and material properties.

In general, various simulations of the crack propagation in the framework of finite element method are available in the literature. The earliest finite element methods based on the Lagrangian formulation use a node release technique for crack propagation [2-4]. Node release technique has the drawbacks of requiring a prior knowledge of the path followed by the crack and also the crack is forced to advance the entire distance between the two nodes of an element edge at each growth step, so the continuous crack tip motion cannot be described. Consequently, it produces inaccurate results and is inappropriate for modeling crack propagation [5].

---

[*] Corresponding author. Tel.: +98 21 84063221; Fax: +98 21 88674748.
  *E-mail addres*s: Shahani@kntu.ac.ir (A. R. Shahani).

The updated Lagrangian formulation can be extended with a remeshing technique by which the old mesh is replaced by a completely new mesh. In fracture study with this technique, the crack growth increment causes the new mesh generation of the model to represent the current crack configuration [6,7]. This means that the mesh topology should be changed frequently during the analysis. So, the crack growth increment is no longer constrained by the old mesh size as in node release technique. However, a search algorithm and interpolation of the state variables to the new mesh is required at each step to complete the solution. Shahani and Seyyedian [8] employed the remeshing to simulate the glass cutting with the impinging hot air jet, in which a controlled crack growth due to the thermal stresses is studied. Rethore et al. [9] presented a stable numerical scheme for simulation of the dynamic crack propagation with the remeshing, however, the aim of their work was not to develop an efficient remeshing procedure. In principle, their study focused on the stability and in their computations, the crack speed has been calculated via the energy release rate considering that the material toughness is independent of the crack speed. Recently, the dynamic crack propagation problem was investigated by using a remeshing technique by Shahani and Amini [10]. Dynamic fracture path prediction in impact fracture phenomena was carried out based on the Delaunay mesh generation scheme applied in each crack growth increment by Nishioka et al. [11].

On the other hand, the Arbitrary Lagrangian Eulerian (ALE) formulation can also be applied to the finite element method to simulate the problems of crack propagation. This can alleviate many of the drawbacks of Lagrangian formulation. The fundamental idea in ALE is to allow the computational mesh to move in an arbitrary manner, independent of the material motion. Subsequently, it is possible to control the mesh motion of a purely Lagrangian formulation or the boundary tracking of a purely Eulerian formulation. Contrary to the remeshing procedure, the mesh topology, i.e., the number of elements and their connectivity is preserved in ALE method. Moreover, the algorithm of the transfer of state variables between the old mesh and the new mesh is more accurate in ALE, where the convection equation is treated.

The ALE formulation of continuum mechanics was originated from the fluid dynamics problems [12, 13]. It was then applied to the nonlinear solid mechanics with path-dependent materials by Liu et al. [14,15]. Huerta and Casadei [16] employed the ALE in large deformation non-linear analysis involving necking and transient punch indentation processes. Gadala and Wang [17−19] applied the ALE formulation in finite strain deformation problems consists of the rate-dependent and rate-independent materials. The stress update procedures in ALE description of non-linear solid mechanics were discussed by Rodriguez-Ferran et al. [20] for transient and quasi static processes. The ALE finite element simulation of three dimensional large deformation problems was performed by Aymone et al. [21]. Rodriguez-Ferran et al. [22] employed the ALE method with hyperelastic-plastic constitutive models to simulate the necking, coining and powder compaction problems. A fully coupled ALE method was presented for large deformation problems by Bayoumi and Gadala [23]. An uncoupled ALE formulation has been employed by Khoei et al. [24] in plasticity behavior of pressure-sensitive materials, with the special reference to large deformation analysis of powder compaction process.

The guidelines for designing effective mesh motion strategies in ALE analysis of particular problems were given by Movahhedy [25] and Gadala et al. [26], and the critical role of mesh motion in the success of ALE analysis was described. The difficult deformation processes such as coining, crack growth and orthogonal metal cutting were presented to demonstrate the capability of ALE formulation and suitable mesh motion techniques. In their study, the numerical schemes were also proposed for moving boundary and interior nodes of a region consistent with the ALE principles. Moreover, the multi region strategy was introduced in mesh motion scheme for the simulation of metal cutting process. This approach is employed in this study for the dynamic fracture simulation.

Ponthot and Belytschko [27] employed ALE in element-free Galerkin (EFG) method to solve one dimensional wave propagation and two dimensional propagating cracks with the constant velocity in an infinite body. Their study was presented for a linear elastic model. A coupled ALE finite element method for simulating two dimensional crack propagation was presented by Gadala [28]. However, the presented ALE methodology uses the special techniques to control the motion of nodes on free boundaries for simulating the crack propagation. The crack propagation problem running at a uniform velocity in an infinite body was simulated by the presented methodology.

The motivation for this study is to present an efficient ALE formulation in the framework of finite element method for the simulation of dynamic crack propagation problem. The three dimensional solution of the problem is performed in this study. The mesh topology is preserved during the crack propagation with the presented ALE algorithm. The crack velocity and crack growth increment is not prescribed and must be predicted using a dynamic fracture criterion. The crack arrest condition is also investigated. This study also does not have the limitation of dynamic crack propagation in the infinite models. The operator splitting technique is used to treat the convective terms of ALE formulation. So, each time step is decoupled into a Lagrangian phase followed by an Eulerian phase. An unconditionally stable and second order accuracy time integration method is employed to solve the dynamic problem. The new surfaces generated by the crack extension are controlled through the mesh motion part of each

ALE step. The isoparametric mapping technique is proposed to implement the mesh motion part, which demonstrates to be very suitable and efficient for the crack growth study. The solution variables are remapped to the relocated mesh using the convection equation. The crack tip motion is governed by a criterion that relates the dynamic stress intensity factor to the dynamic fracture toughness of the material. The different stages of modeling are applied to a finite element code, which is conducted by ANSYS parametric design language (APDL) [29]. The presented ALE algorithm can be used for both structured and unstructured meshes. The prepared ALE finite element code is easily applicable to simulate self similar dynamic crack propagation. The parameters such as the history of crack velocity, dynamic stress intensity factor and energy quantities are computed and are validated with the experimental study. The comparison is also made between the crack velocity predicted in the present study and that obtained via the remeshing technique cited in the literature. It is seen that the ALE formulation is a powerful alternative method by combining the advantages of both Lagrangian and Eulerian formulation for the dynamic crack propagation process.

2 THE ALE FORMULATION
2.1 ALE kinematics

Two domains are commonly employed in continuum mechanics: the material domain Ω_X, made up of material particles X, and the spatial domain Ω_x, consisting of the spatial points x. The ALE formulation considers a third domain that is the referential configuration, Ω_χ, formed by the reference (or grid) points χ in addition to the material and spatial domains. A convenient way to provide one-to-one transformations between the three domains is by means of the equations of material motion and referential motion that is also known as the mesh motion [28, 30]. The material motion is defined by $x = \phi(X,t)$ and the mesh motion is defined by $x = \hat{\phi}(\chi,t)$. Generally, the motion of the referential coordinate point χ is arbitrary and thus it does not coincide with the material coordinates.

The material velocity $\mathbf{v}$ and the mesh velocity $\hat{\mathbf{v}}$ are determined by differentiating the equations of material motion and mesh motion with respect to time while keeping the material coordinate X or the grid point χ fixed [30]:

$$\mathbf{v} = \frac{\partial \boldsymbol{x}}{\partial t}\bigg|_X = \frac{\partial \phi(X,t)}{\partial t}\bigg|_X \tag{1}$$

$$\hat{\mathbf{v}} = \frac{\partial \boldsymbol{x}}{\partial t}\bigg|_\chi = \frac{\partial \hat{\phi}(\chi,t)}{\partial t}\bigg|_\chi \tag{2}$$

The difference between the material and mesh velocity is introduced as convective velocity $(c = \mathbf{v} - \hat{\mathbf{v}})$ that represents the velocity of material particles relative to grid points. Although the two velocities are in general independent from each other, there exists a one-to-one mapping between them. At any given time each grid point should coincide with one and only one material point, provided that the Jacobian of the mapping function is non-zero. In addition, the boundary constraint, which ensures that the material and grid configurations have the same boundary at all times, can be expressed in the form [28]:

$$(\mathbf{v} - \hat{\mathbf{v}}).\boldsymbol{n}^b = 0 \tag{3}$$

where $\boldsymbol{n}^b$ represents the normal vector to the boundary and (·) represents the scalar product of the vectors. The physical interpretation of Eq. (3) is that no normal convective velocity occurs across the boundary if the boundary particles remain on the boundary.

The governing ALE equations involve the material time derivative of some quantities. For a given arbitrary vector function f_i, the material derivative denoted by $\dot{f}_i$ is defined to be the rate of changes of the function holding the material particle X fixed. The referential time derivative denoted by f' is also the time derivative of function f_i holding the reference point χ fixed. The relationship between the material time derivative and referential time derivative of an arbitrary vector function f_i is given by the convective derivative [12, 30] as

$$\dot{f}_i = \left.\frac{Df_i}{Dt}\right|_X = \left.\frac{\partial f_i}{\partial t}\right|_\chi + c_j \frac{\partial f_i}{\partial x_j} = f_i' + c.\nabla f_i \tag{4}$$

The term $c \cdot \nabla f_i$ in Eq. (4) represents the convective effects, which means that the material particle X is neither attached to the spatial point x nor to the grid point χ.

2.2 Governing equations of the problem

The balance of momentum equation for the dynamic problems in the updated Lagrangian description is

$$\frac{\partial \sigma_{ji}}{\partial x_j} + \rho b_i = \rho \dot{\mathbf{v}}_i \tag{5}$$

where σ_{ji} is the Cauchy stress tensor and b_i is the body force. The right-hand side of Eq. (5) expresses the inertia force with the mass density, ρ, and material time derivative of velocity $\mathbf{v}_i$. In ALE description, the governing equations can be derived by applying the convective derivative relation, i.e., Eq. (4), into the continuum mechanics governing equations. Thus, the balance of momentum equation in ALE formulation can be readily obtained as [30]

$$\frac{\partial \sigma_{ji}}{\partial x_j} + \rho b_i = \rho\left(\mathbf{v}_i' + c.\nabla \mathbf{v}_i\right) \tag{6}$$

where v_i' is the referential acceleration and $\nabla \mathbf{v}_i$ is the velocity gradient tensor. The Cauchy stress tensor in Eq. (6) is obtained from the isotropic linear elastic constitutive equation written as

$$\sigma_{ij} = \frac{E}{1+v}\left(\varepsilon_{ij} + \frac{v}{1-2v}\varepsilon_{kk}\delta_{ij}\right) \tag{7}$$

where v and E are the elastic constants, δ_{ij} is the Kronecker delta and ε_{ij} is the strain tensor that follows the small displacement rule.

As, in this study the path I ndependent material is studied, the constitutive equation does not have the rate form. Hence, no convective terms are introduced in the constitutive governing equation. However, the convective term $c.\nabla \mathbf{v}_i$ in the momentum equation, i.e., Eq. (6) should be taken into account [20, 30].

3 NUMERICAL TREATMENTS

In this study, the uncoupled ALE approach is used to deal with the numerical implementation of Eq. (6). Hence, an operator splitting technique is applied to treat the material and convective effects separately [30]. In this approach, as shown in Fig. 1, every time step is decomposed into a Lagrangian phase followed by an Eulerian phase. The advantage of the operator splitting technique proposed by Benson [31] and Ponthot and Hogge [32] is that the calculations are performed in the Lagrangian phase with no convective term to achieve the equilibrium. Such a technique has been applied to finite element method to solve the forming problems in solid mechanics [20-22, 24, 25, 33-35].
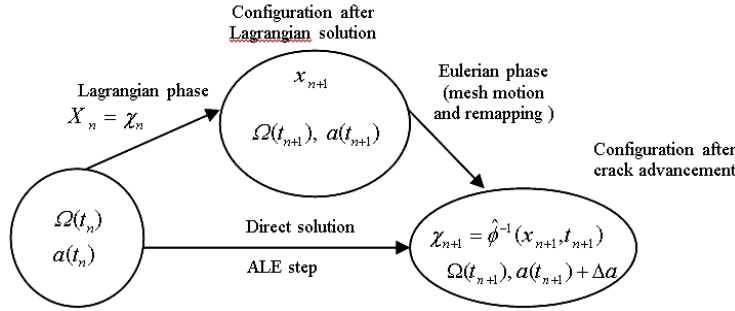
Fig. 1
Decomposition of each ALE step into a Lagrangian phase and Eulerian phase.

3.1 Lagrangian (material) phase

The first phase of the operator split is to implement a pure Lagrangian procedure without considering the convective effects. So, the mesh is attached to the material, i.e., the material and referential coordinate systems are the same ($X=\chi$). Consequently, the convective effects in Eq. (6) are neglected ($c=0$) and it simplifies to Eq. (5). The finite element equations for the updated Lagrangian formulation are developed by means of the virtual work. To this task, the weak form of Eq. (5) can be obtained by multiplying it by kinematically admissible test function δu_i over the current domain Ω_x [30], which using the integration by part and applying the divergence theorem yields

$$\int_{\Omega_x} \rho \, \delta u_i \left. \frac{\partial^2 u_i}{\partial t^2} \right|_X d\Omega_x + \int_{\Omega_x} \frac{\partial(\delta u_i)}{\partial x_j} \sigma_{ji} \, d\Omega_x = \int_{\Omega_x} \rho \delta u_i b_i \, d\Omega_x + \int_{\Gamma_t} \delta u_i t_i \, d\Gamma_t \tag{8}$$

where u_i represents the displacement field and Γ_t refers to the part of the boundary on which the traction force $t_i=\sigma_{ij}n_j$ is prescribed. Prefix δ designates an arbitrary, virtual and compatible variation. After finite element discretization of the body, virtual nodal displacements are eliminated from Eq. (8) and it can be rewritten as the set of second order ordinary differential equations [30]:

$$M\ddot{\mathbf{u}} + K\mathbf{u} = \boldsymbol{F}^{ext} \tag{9}$$

where

$$M = \int_{\Omega_x} \rho \boldsymbol{N}^T \boldsymbol{N} d\Omega_x \tag{10}$$

$$K = \int_{\Omega_x} \boldsymbol{B}^T \boldsymbol{D} \boldsymbol{B} \, d\Omega_x \tag{11}$$

$$\boldsymbol{F}^{ext} = \int_{\Omega_x} \rho \boldsymbol{N}^T \boldsymbol{b} \, d\Omega_x + \int_{\Gamma_t} \boldsymbol{N}^T \boldsymbol{t} \, d\Gamma_t \tag{12}$$

where M is the mass matrix, K the stiffness matrix, $\boldsymbol{F}^{ext}$ the external force vector acting on the finite element nodes and $\ddot{\mathbf{u}}$ represents the nodal acceleration vector. N is the shape function matrix and superscript T indicates the matrix transpose. It should be noted that the mass, stiffness and external force matrices are recomputed at the beginning of each time step since the domain of the problem is changed as the crack propagates.

The governing Eq. (9), which is associated with the prescribed initial conditions $\mathbf{u}_n$ and $\mathbf{v}_n$ at the beginning of current time step $\Delta t_n=t_{n+1}-t_n$, can be solved for time t_{n+1}. The implicit time integration procedure by using the Newmark Eqs. [36, 37] is employed to solve the dynamic problem represented by Eq. (9). Accordingly, the unknown values at time t_{n+1}, i.e., $\mathbf{u}_{n+1}$, $\mathbf{v}_{n+1}$ and $\ddot{\mathbf{u}}_{n+1}$ are computed solving the following algebraic system of equations:

$$M\ddot{\mathbf{u}}_{n+1} + K\mathbf{u}_{n+1} = \boldsymbol{F}^{ext} \tag{13}$$

$$\boldsymbol{u}_{n+1} = \boldsymbol{u}_n + \Delta t_n \mathbf{v}_n + \Delta t_n^2 [(\frac{1}{2} - \alpha)\ddot{\mathbf{u}}_n + \alpha \ddot{\mathbf{u}}_{n+1}] \tag{14}$$

$$\mathbf{v}_{n+1} = \mathbf{v}_n + \Delta t_n [(1 - \gamma)\ddot{\mathbf{u}}_n + \gamma \ddot{\mathbf{u}}_{n+1}] \tag{15}$$

The parameters α and γ appeared in Eqs. (14) and (15) determine the stability and accuracy characteristics of this algorithm. The Newmark method is unconditionally stable and second order accurate for structural dynamic problems when the integration parameters satisfy the relevant relationships [37]. In this study, the values of $\alpha = 0.25$ and $\gamma = 0.5$ are applied into the Eqs. (14) and (15).

3.2 Governing equation of crack motion

For the straight self-similar crack propagation, the computational simulations for a given initial crack length, specimen geometry, and applied load can be conducted in either of two ways. One of these is the generation phase simulation in which the variation of a fracture parameter such as stress-intensity factor can be determined, using an experimentally measured crack propagation history (a or $\dot{a}$ vs. t curve) as the input data into the computational model. On the other hand in the second type of computational simulation, which is called the application phase simulation, the crack propagation history and the crack velocity can be predicted by specifying the material dynamic fracture toughness data as inputs to the computational model. In this study, the application phase type of the computational simulation is used for the dynamic fracture analysis. In this case, for a given dynamic fracture problem, a fracture criterion governing the crack tip motion is required to predict both the instantaneous crack speed $\dot{a}(t)$ and instantaneous crack length $a(t)$. In this study, the crack tip equation of motion is explained by the critical dynamic stress intensity factor criterion [38]. The crack grows in such a way that its tip dynamic stress intensity factor, K^d, is always equal to the dynamic fracture toughness of the material, K_D. The stress intensity factor represents the effect of the applied loading, geometrical configuration, and the parameters of the bulk material around the crack tip region. While, the dynamic fracture toughness represents the resistance of material to the crack growth. It depends on the material properties and can be determined through the laboratory measurement. Hence, the equation of crack tip motion for the purely mode *I* can be written [38] as:

$$K_I^d(a(t), \dot{a}(t), \sigma(t)) = K_D(\dot{a}) \tag{16}$$

It is shown from Eq. (16) that the dynamic stress intensity factor is dependent on the crack length, crack speed and the stress field $\sigma(t)$ due to applied load. According to this criterion, the crack arrest occurs when the crack stress intensity factor is less than the value of crack arrest fracture toughness or crack arrest SIF K_D ($\dot{a} = 0$). The effect of velocity in dynamic stress intensity factor is defined by a separate function and can be written as [38, 39]:

$$K_I^d(a(t), \dot{a}(t), \sigma(t)) = k_I(\dot{a}) K_I^*(a(t), \sigma(t)) \tag{17}$$

where K_I^* is the equilibrium stress intensity factor that depends on the current crack length, the applied load, which both can be time dependent. It has the dimensions of a static stress intensity factor, but it is not equal to the static stress intensity factor for a stationary crack of the same length as the moving crack. The subscript *I* refers to mode *I* of fracture. k_I is a function of crack speed, and can be approximated in the form [38]:

$$k_I(\dot{a}) = \frac{1 - \dot{a}/c_R}{1 - \dot{a}/2c_R} \tag{18}$$

where C_R is the Raleigh wave speed that its value is 975 m/s for Epoxy-Resin [10]. The crack-velocity function k_I is a universal function for all elasto dynamically propagating cracks. When the crack is not propagating ($\dot{a} = 0$), this
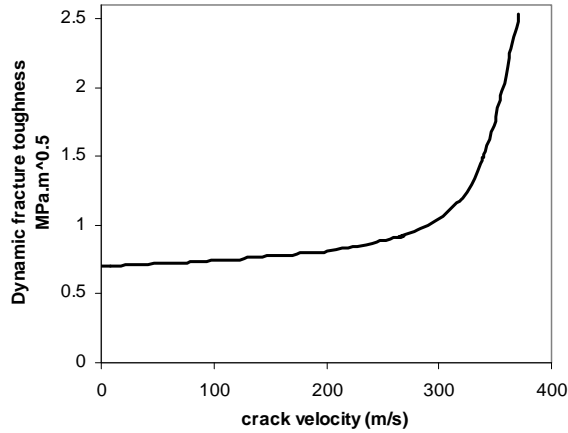
Fig. 2
Dynamic fracture toughness vs. crack velocity for
Araldite-B [43].

function takes a unit value, and decreases monotonically with increasing crack velocity while it reduces to zero when the crack velocity is equal to C_R. Dynamic fracture toughness K_D is a nonlinear material property, which is expected to be dependent on the crack speed in a special temperature and is obtained through the experimental tests [40, 41]. In the current study, the dynamic fracture toughness data of the Araldite-B material reported by Kalthoff et al. [42] and Kanninen and Popelar [43] are used (Fig. 2).

The stress intensity factor K_I^* is computed for the crack front nodes at each time step using the interaction integral method [29]. Thereafter, using the data of material dynamic fracture toughness, the Eq. (16) is solved for the crack velocity at the end of current time step using the Newton-Raphson iterative procedure. The crack growth increment for the next time step Δt_{n+1} is then computed as $\Delta a = \dot{a}\Delta t_{n+1}$.

3.2.1 Interaction integral method

Interaction energy integral is a two state integral which allows the mixed mode stress intensity factors to be computed independently by superimposing suitable auxiliary fields to the actual ones [44]. It is derived from the J-integral by considering a composition of two admissible states. This approach does not require to accurately capture singular fields in the vicinity of crack tip, moreover, it can be easily introduced in the finite element framework [45]. The interaction integral method is briefly discussed here [44, 46].

The local coordinate system are taken to be at the crack tip with the x_1-axis parallel to the crack faces and is pointed to the crack extension, the x_2-axis is pointed to the normal of the crack surfaces or edges, and the x_3-axis pointed to the tangential direction of the crack front, as shown in Fig. 3. Two states of the cracked body are considered. State 1, $\left(\sigma_{ij}^{(1)}, \varepsilon_{ij}^{(1)}, u_{ij}^{(1)}\right)$, corresponds to the actual state and state 2, $\left(\sigma_{ij}^{(2)}, \varepsilon_{ij}^{(2)}, u_{ij}^{(2)}\right)$, is an auxiliary state which is chosen as the asymptotic fields for different fracture modes [44]. So, the interaction integral is written as

$$I^{(1,2)} = \int_{\Gamma} \left[\sigma_{mn}^{(1)} \varepsilon_{mn}^{(2)} \delta_{1j} - \sigma_{ij}^{(1)} \frac{\partial u_i^{(2)}}{\partial x_1} - \sigma_{ij}^{(2)} \frac{\partial u_i^{(1)}}{\partial x_1} \right] n_j \, \mathrm{d}\Gamma \qquad (19)$$

For the sake of simplicity for numerical computation, the interaction integral (19) is written in the domain form as

$$I^{(1,2)} = \int_{V} \left[\sigma_{ij}^{(1)} \frac{\partial u_i^{(2)}}{\partial x_1} + \sigma_{ij}^{(2)} \frac{\partial u_i^{(1)}}{\partial x_1} - \sigma_{mn}^{(1)} \varepsilon_{mn}^{(2)} \delta_{1j} \right] \frac{\partial q}{\partial x_j} \, \mathrm{d}V \qquad (20)$$

The domain form interaction integral (20) is calculated over the volume V, including a group of elements to be surrounded by a contour Γ_A (Fig. 3). q is referred to as the crack extension vector. The direction of q is the simple x_1-axis of the local coordinate system ahead of the crack tip. The q vector is chosen as zero at nodes along the contour, and is a unit vector for all nodes inside the contour. For a given node on the crack front, the finite element mesh corresponding to the finite domain V over which the domain integral is defined is shown in Fig. 3 for an arbitrary contour Γ_A illustrated by the thick lines. This domain is defined by sweeping the Area A, surrounded by contour Γ_A, along the segment Δ. The size of the domain is dominated by the size of contour. The local coordinate system associated with the considered crack front node is also shown in Fig. 3. According to Fig. 3, the crack plane normal is the x_2-axis of the defined local coordinate system.

The interaction integral $I^{(1,2)}$ is associated with the various modes of stress-intensity factor as

$$I^{(1,2)} = \frac{2(1-v^2)}{E}\left(K_I^{(1)}K_I^{(2)} + K_{II}^{(1)}K_{II}^{(2)}\right) + \frac{2(1+v)}{E}K_{III}^{(1)}K_{III}^{(2)} \tag{21}$$

where $K_I^{(1)}$, $K_{II}^{(1)}$ and $K_{III}^{(1)}$ are the mode I, II and III stress intensity factors and $K_I^{(2)}$, $K_{II}^{(2)}$ and $K_{III}^{(2)}$ are the auxiliary mode I, II and III stress intensity factors. In a problem that all the three modes are produced, by choosing the three different auxiliary fields, each stress intensity factor can be calculated independently. In this study, the out of plane loading is absent. So, the value of K_{III} is zero. The mode II stress intensity factor is also eliminated, since both the geometry and loading are symmetrical. Thus, the auxiliary field is so selected that $K_I^{(2)} = 1$, then the value of $K_I^{(1)}$ is obtained from Eq. (21) as

$$K_I^{(1)} = \frac{E}{2(1-v^2)}I^{(1,2)} \tag{22}$$

It is noteworthy that the employed time step Δt_n is sufficiently small during the finite element solution of system of Eqs. (13)-(15). Nevertheless, each time step Δt_n is subdivided into 50 substeps to achieve dynamic equilibrium using the implicit time integration.

3.3 Eulerian phase

The second phase of the operator splitting, which is the Eulerian phase deals with the convective terms that have not been taken into account during the Lagrangian phase and consists of two parts:

3.3.1 Mesh motion

In the crack propagation problem, the mesh motion strategy is to create the traction free surface owing to crack advancement. As shown in Fig. 4(a) because of symmetry, one half of the DCB is modeled by FEM. The idea of mesh motion is taken from the isoparametric mapping method, which was originally proposed by Zienkiewicz and Phillips [47] for the mesh generation.
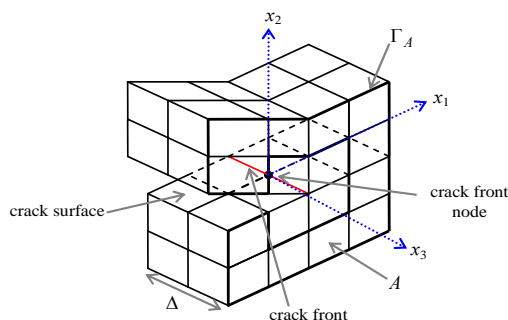

Fig. 3
Details of the finite element mesh corresponding to the finite domain V over which the domain integral is defined, the defined local coordinate system at the considered crack front node. Note that the domain V is defined by sweeping the Area A, surrounded by contour Γ_A, along the segment Δ.

The use of isoparametric mapping method was advocated by Movahhedy [25, 26] for mesh motion in ALE analyses. Following the mesh motion scheme presented by Movahhedy [25, 26] for the 2D simulation of metal cutting process, the model is subdivided into different regions as shown in Fig. 4(a): the purely Lagrangian region including the loading point, the central region including the crack tip and the left and right ALE regions. The central region with the fixed mesh size moves with the crack velocity during the analysis. All external boundaries are Lagrangian in the normal direction according to the ALE boundary constraint (3).

For a given initial mesh, the first step is to find the parametric coordinates (P_r, P_s) of all nodal points of the model regions. Thus, each region can be considered as a super element with four straight sides and four corner nodes. As the mesh motion does not occur in thickness direction, the corresponding equations are considered just in x and y directions. So, the parametric coordinates of each internal or boundary node in each region can be obtained solving the nonlinear equations given by

$$(\sum_{i=1}^{4} P_{ri} x_i)P_r + (\sum_{i=1}^{4} P_{si} x_i)P_s + (\sum_{i=1}^{4} P_{ri} P_{si} x_i)P_r P_s = 4x - \sum_{i=1}^{4} x_i \tag{23}$$

$$(\sum_{i=1}^{4} P_{ri} y_i)P_r + (\sum_{i=1}^{4} P_{si} y_i)P_s + (\sum_{i=1}^{4} P_{ri} P_{si} y_i)P_r P_s = 4y - \sum_{i=1}^{4} y_i \tag{24}$$

where x_i, y_i are the global coordinates of the corner nodes of each region, and P_{ri} and P_{si} are their local coordinates. The subscript 'i' refers to the number of corner nodes and x, y are the global coordinates of internal nodes. The parametric coordinates P_r, P_s of the nodes in each region are computed by solving Eqs. (23) and (24) only once at the beginning of analysis, and the computed values are stored. Once the crack tip motion was determined in each time step, the coordinates of corner nodes in each region are updated. Next, with the aid of computed parametric coordinates, the new coordinates of each internal or boundary nodes of each region can be calculated using the direct mapping written by

$$x^{new} = \sum_{i=1}^{4} N_i(P_r, P_s) x_i^{new}, \qquad y^{new} = \sum_{i=1}^{4} N_i(P_r, P_s) y_i^{new} \tag{25}$$

The mesh velocity of each node can now be computed using the new nodal coordinates. Fig. 4(a) illustrates the generated finite element mesh according to the initial crack length with the symmetry boundary condition at the lower edge of the model. Fig. 4(b),4(c) and 4(d) also show the mesh topology and deformed shape of the model during the mode *I* crack propagation with the proposed ALE analysis.

(a)

(b)

(c)
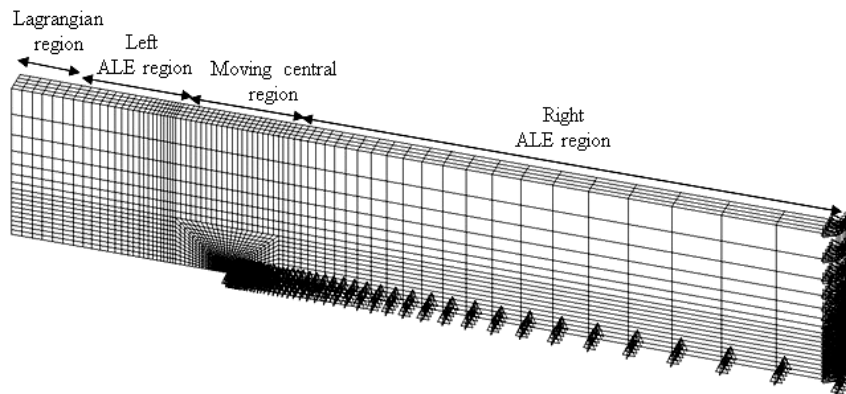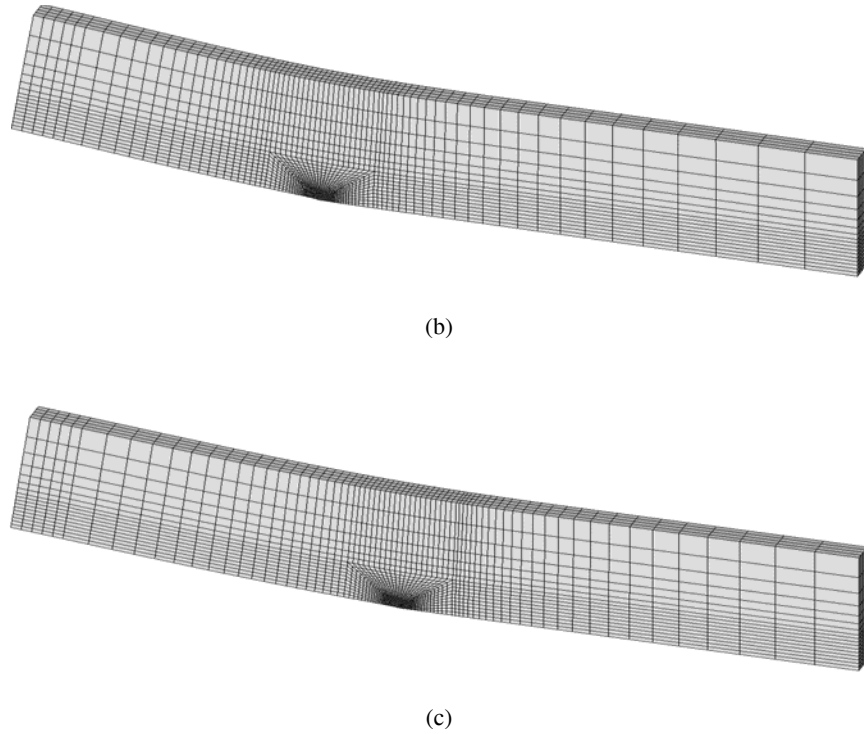
Fig. 4
3D FE model and its boundary conditions; (a) initial generated mesh in different regions; (b) pattern of moving mesh and deformation after 25 mm crack propagation; (c) pattern of moving mesh and deformation after 57 mm crack propagation.

3.3.2 Transport process

The ALE step in the uncoupled approach is completed with a transport or convection process. This means that after the mesh motion in each time step, all the state variables have to be remapped from the Lagrangian solution to the relocated mesh according to the convection algorithm. The number of variables to be remapped will depend on the material constitutive model. However, in dynamic problems, the inertia effects should also be taken into account during the ALE step analysis, which leads to transferring of the velocity field. The remapping of state variables consists of solving the classical convection equation, which can be written as [20, 30]:

$$\frac{\partial \beta}{\partial t}\bigg|_{\chi} + c_j \frac{\partial \beta}{\partial x_j} = 0 \tag{26}$$

The Eq. (26) is resulted from the convective derivative relation (4) with $\left(D\beta/Dt\right)\big|_{X} = 0$, since this term was accounted for in Lagrangian phase [20, 30]. The variable β may be the displacement, stress or velocity field.

As the mesh motion is carried out at each time step, the Lagrangian mesh is close to the relocated (Eulerian) mesh. Accordingly, by applying Eq. (26) into the first order Taylor series expansion [30, 32, 34], yields a sufficiently accurate relation between the unknown value of solution variable at the new mesh and the value obtained at the Lagrangian mesh:

$$\beta_i^{\mathbf{E}} = \beta_i^{\mathbf{L}} - \Delta t\, \mathbf{c} \cdot \nabla \beta_i = \beta_i^{\mathbf{L}} - \Delta t\, c_j \frac{\partial \beta_i}{\partial x_j} \tag{27}$$

where $\beta^{\mathbf{E}}$ is the value of state variable for the relocated nodes to be found, $\beta^{\mathbf{E}}$ is the corresponding Lagrangian solution and $\nabla \beta$ is the gradient tensor of that variable. Here, the gradient tensor of a variable is evaluated at the

material points. The gradient tensor components of a variable at each material point with the given coordinate $\boldsymbol{x}$ are calculated by

$$\left.\frac{\partial \beta_i}{\partial x_j}\right|_x = \frac{1}{m}\sum_{k=1}^{m}\sum_{I=1}^{n}\left(\left.\frac{\partial N_I(r,s)}{\partial x_j}\right|_x \beta_{iI}^{\mathbf{L}}\right) \tag{28}$$

where $_j$ refers to the x, y or z component, n is the number of nodes per element, $N_I (r,s)$ is the shape function expressed by the element coordinates r and s and $\beta_I^{\mathbf{L}}$ is a state variable at Lagrangian node I. Also, m refers to the number of elements connected to the considered node. The spatial derivative of shape functions are calculated as [35, 37]

$$\begin{Bmatrix} \dfrac{\partial N_I}{\partial x_1} \\[2mm] \dfrac{\partial N_I}{\partial x_2} \\[2mm] \dfrac{\partial N_I}{\partial x_3} \end{Bmatrix} = \boldsymbol{J}^{-1}\begin{Bmatrix} \dfrac{\partial N_I}{\partial r} \\[2mm] \dfrac{\partial N_I}{\partial s} \\[2mm] \dfrac{\partial N_I}{\partial t} \end{Bmatrix} \tag{29}$$

In above relation, $\boldsymbol{J}^{-1}$ is the inverse of the Jacobian matrix. The Jacobian matrix is written as [35]

$$\boldsymbol{J} = \begin{vmatrix} \displaystyle\sum_{I=1}^{n}\frac{\partial N_I}{\partial r}x_{1I} & \displaystyle\sum_{I=1}^{n}\frac{\partial N_I}{\partial r}x_{2I} & \displaystyle\sum_{I=1}^{n}\frac{\partial N_I}{\partial r}x_{3I} \\[4mm] \displaystyle\sum_{I=1}^{n}\frac{\partial N_I}{\partial s}x_{1I} & \displaystyle\sum_{I=1}^{n}\frac{\partial N_I}{\partial s}x_{2I} & \displaystyle\sum_{I=1}^{n}\frac{\partial N_I}{\partial s}x_{3I} \\[4mm] \displaystyle\sum_{I=1}^{n}\frac{\partial N_I}{\partial t}x_{1I} & \displaystyle\sum_{I=1}^{n}\frac{\partial N_I}{\partial t}x_{2I} & \displaystyle\sum_{I=1}^{n}\frac{\partial N_I}{\partial t}x_{3I} \end{vmatrix} \tag{30}$$

4   RESULTS AND DISCUSSION

The presented algorithm is applied to solve the dynamic crack propagation problem in the DCB sample under fixed displacement loading. The through-thickness crack is treated. The mode I self-similar dynamic crack propagation is investigated in this study. The assumption of straight crack front is applied to the problem simulation during the crack propagation. Fig. 5 depicts a DCB specimen geometry, which is employed in this study. The dimensions of the specimen are given in millimeters as follows [42]: length L=321, initial crack length a_0=67.8, beam height h=63.5, distance from beam end to pin e=16, distance from crack plane to pin b=20 and thickness B=10. The mechanical properties of Araldite-B are also given in Table 1, which are slightly different in static and dynamic cases [42]. In this study, the dynamic material properties are employed in the analysis. The isotropic linear elastic constitutive model is employed in dynamic crack propagation analysis of Araldite-B, which is a brittle material.
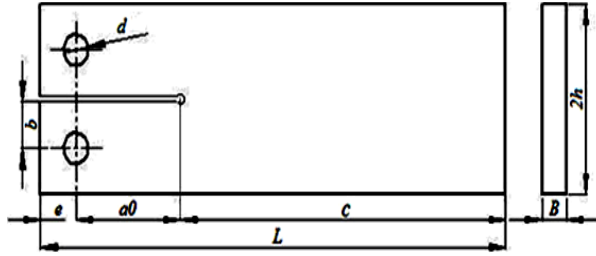
Fig. 5
Geometry of the DCB specimen.

Table 1
Mechanical properties of material [42].

Epoxy-Resin	E (GPa)	v	ρ (kg/m^3)
Dynamic	3.66	0.39	1172
Static	3.38	0.33	1172

The FE model of the problem is shown in Fig. 4. Eight-node 3D element (Solid185) is employed in the analysis [29]. The element, its nodes location and the employed local coordinate system in element formulation is shown in Fig. 6. This element has three degrees of freedom at each node that are nodal translations in the *x*, *y* and *z* directions. The finite element analysis is performed by using a mesh contains 5068 3D elements and 6775 nodes.

The simulation is carried out for the specimen with the initiation stress intensity factor K_q=1.33MPa.m$^{0.5}$ [42]. The crack propagation is initiated in the specimen with the initial crack length, by increasing the vertical displacement at the pin location until the crack stress intensity factor reaches its critical value K_q. Thereafter, the pin displacement is held fixed throughout the simulation. Four elements are used in the thickness direction. As mentioned, the crack front has the straight profile during the crack propagation in this study. However, in high velocities crack propagation, the straight crack front is observed in the experimental works [48]. Furthermore, using the BEM method, it is predicted that for high crack velocity of dynamic crack propagation, the crack front maintains its straight profile [49].

The crack tip equation of motion, i.e., Eq. (16) is solved at each time step and the corresponding results are illustrated in the following. The predicted crack propagation velocity vs. time is represented in Fig. 7, and is compared with the experimental results reported by Kalthoff et al. [42]. To check the accuracy of the presented algorithm, the computed crack velocity from our previous work on the remeshing technique [10] is also shown in Fig. 7. Accordingly, the predicted crack propagation velocity from the presented ALE algorithm in this study shows more agreement with the experimental work in comparison with those obtained via the remeshing technique. The arrest time is also better estimated in this study. So, using the ALE method and its capability in mesh motion scheme, the dynamic crack propagation is simulated with the computational saving and more accuracy in the results. The history of computed dynamic stress intensity factor along the crack front from Eq. (17) is shown in Fig. 8. It is observed that the maximum values of computed dynamic stress intensity factor during the crack propagation are related to the deepest point of the crack front. However, the value of dynamic stress intensity factor reduces near the free surfaces (corner nodes) of the specimen. This agrees with the reported BEM analysis by Agrawal [49] for the through-thickness straight running crack. The determined dynamic stress intensity factor in this study is shown that is in good agreement with the experimental results of Kalthoff et al. [42].
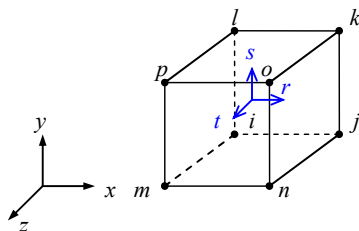

Fig. 6
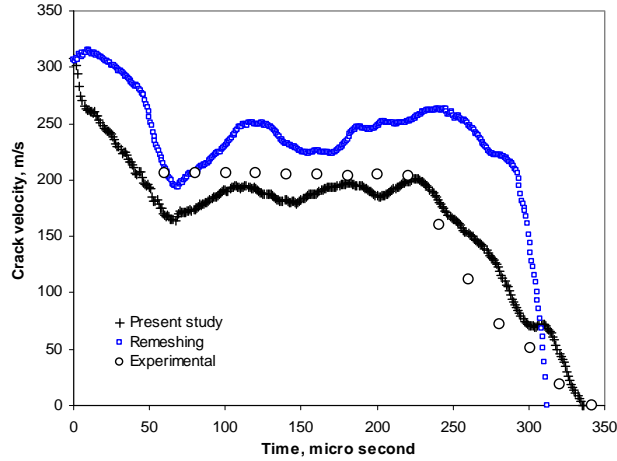Geometry of the employed eight-node 3D element and its nodes location.

Fig. 7
The variation of crack propagation velocity vs. time for DCB specimen with K_q=1.33MPa.m$^{0.5}$.
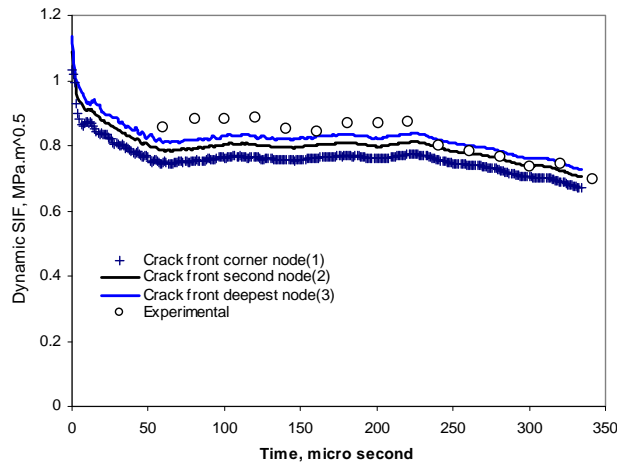

Fig. 8
The variation of dynamic stress intensity factor along the crack front vs. time for DCB specimen.
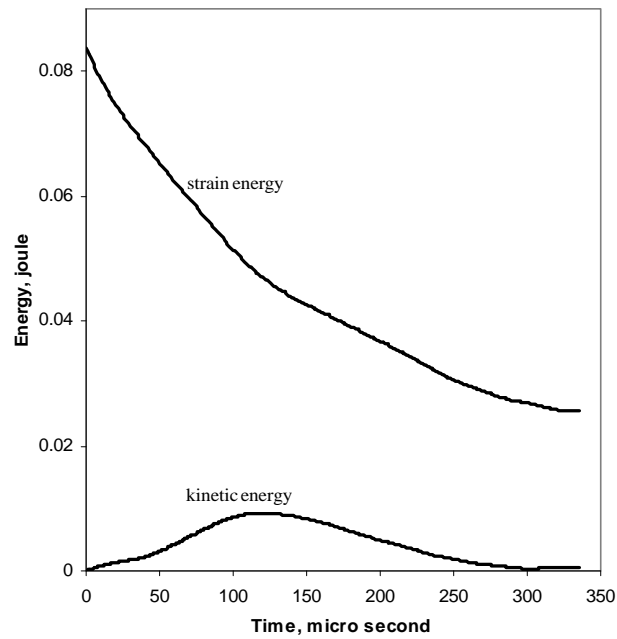

Fig. 9
The kinetic and strain energy values during dynamic fracture for DCB specimen under fixed displacement conditions.
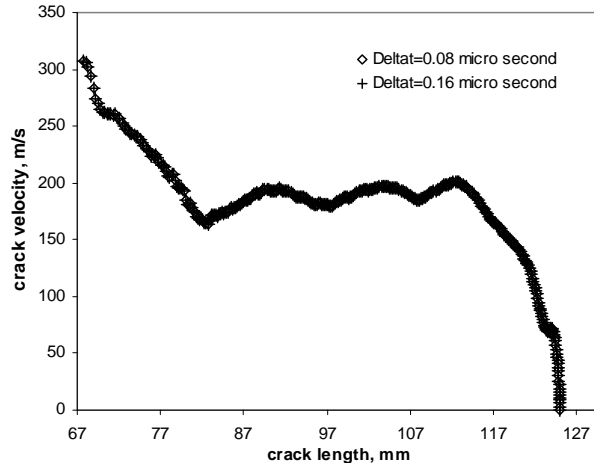
Fig. 10
Study of the solution convergence based
on the predicted crack velocity.

The variations of strain energy and kinetic energy of the model are shown in Fig. 9 as a function of time. It is seen that the maximum strain energy corresponds to the beginning of the process when the stress intensity factor has its maximum value. Afterward, as the crack propagates the strain energy of the model decreases. This is due to the fixed displacement condition. The minimum value of strain energy corresponds to the crack arrest time. The kinetic energy of the specimen begins with the zero value at the start of the solution and reaches a maximum value after a specified propagated crack length and finally tends to zero at the crack arrest time.

The reported crack arrest length by Kalthoff et al. [42] is 129.5mm and the predicted value in this study is 125mm. The convergence of the solution is also checked and is shown in Fig. 10 through the predicted crack velocity. To this task, the crack velocity is computed at two different time steps, i.e., Δt_n=0.08 and 0.16μs. The corresponding results coincide with each other, which confirm the convergence.

5 CONCLUSION

This paper aimed at elucidating the powers of the ALE finite element method to simulate the self-similar dynamic crack propagation. To treat the convective terms appeared in the ALE formulation, each time step of the solution is decoupled into an updated Lagrangian phase followed by an Eulerian phase. In Lagrangian phase, the implicit time integration method with the unconditionally stable and second order accurate method is applied to the dynamic problem. The mesh motion process based on the isoparametric mapping method is proposed here. It is shown that this mesh motion technique can be very suitable and computationally efficient for crack growth studies. With the organized mesh motion process, a regular and a high resolution mesh at the moving crack tip can be maintained during the simulation with no change in number of elements. During the problem solution neither new nodes nor new elements are created. A proper manner was presented to treat the convective effects in dynamic finite element analysis by which the convergence of the solution can be easily obtained. The nonlinear equation of crack tip motion is governed by the critical dynamic stress intensity factor criterion, and is solved for the crack velocity. The variation of dynamic stress intensity factor along the crack front is also investigated. The obtained results are validated with the experimental study. In comparison with the results of remeshing approach, a more agreement is seen between the predicted crack velocity via the present study and the experimental work. So, it can be noticed that the ALE formulation is more robust and a good alternative in terms of the accuracy and efficiency by combining the advantages of both Lagrangian and Eulerian approaches for the dynamic crack propagation study.

REFERENCES

[1]   Shahani A.R., Amini M.R., 2010, Analytical modeling of dynamic fracture and crack arrest in DCB specimens under fixed displacement conditions, *Fatigue and Fracture of Engineering Materials and Structures* **33**(7): 436-451.

[2]   Yagawa G., Sakai Y., Ando Y., 1977, Analysis of a rapidly propagating crack using finite elements, in: *Fast Fracture and Crack Arrest*, edited by G.T. Hann, M.F. Kanninen, ASTM special technical publication **627**: 109-122.

[3]   Keegstra P.N.R., Head J.L., Turner C.E., 1978, A two dimensional dynamic linear elastic finite element program for the analysis of unstable crack propagation and arrest, in: *Numerical Methods in Fracture Mechanics, Proceedings of the 1st International Conference*, Swansea, Wales, United Kingdom, 634-647.

[4]   Caldis E.S., Owen D.R.J., Zienkiewicz O.C., 1979, Nonlinear dynamic transient methods in crack propagation studies, in: *Nonlinear and Dynamic Fracture Mechanics*, edited by N. Perrone, S.N. Atluri, ASME Applied Mechanics Division, New York, **35**: 1–17.

[5]   Kanninen M.F., 1978, A critical appraisal of solution techniques in dynamic fracture mechanics, in: *Numerical Methods in Fracture Mechanics*, edited by A.R. Luxmore, D.R.J. Owen, Pineridge Press, Swansea, United Kingdom, 612-633.

[6]   Swenson D.V., Ingraffea A.R., 1988, Modeling mixed-mode dynamic crack propagation using finite elements, *Theory and Applications, Computational Mechanics* **3**(6): 381-397.

[7]   Wawrzynek P.A., Ingraffea A.R., 1989, An interactive approach to local remeshing around a propagating crack, *Finite Elements in Analysis and Design* **5**(1): 87-96.

[8]   Shahani A.R., Seyyedian M., 2004, Simulation of glass cutting with an impinging hot air jet, *International Journal of Solids and Structures* **41**: 1313-1329.

[9]   Rethore J., Gravouil A., Combescure A., 2004, A stable numerical scheme for the finite element simulation of dynamic crack propagation with remeshing, *Computer Methods in Applied Mechanics and Engineering* **193**(44): 4493-4510.

[10]   Shahani A.R., Amini M.R., 2009, Finite element analysis of dynamic crack propagation using remeshing technique, *Journal of Materials and Design* **30**(4): 1032-1041.

[11]   Nishioka T., Tokudome H., Kinoshita M., 2001, Dynamic fracture-path prediction in impact fracture phenomena using moving finite element based on Delaunay automatic mesh generation, *International Journal of Solids and Structures* **38**(30-31): 5273-5301.

[12]   Hughes T.J.R., Liu W.K., Zimmermann T.K., 1981, Lagrangian Eulerian finite element formulation for incompressible viscous flows, *Computer Methods in Applied Mechanics and Engineering* **29**(3): 329-349.

[13]   Kennedy J.M., Belytschko T., 1981, Theory and application of a finite element method for arbitrary Lagrangian-Eulerian fluids and structures, *Nuclear Engineering and Design* **68**(2): 129-146.

[14]   Liu W.K., Belytschko T., Chang H., 1986, An arbitrary Lagrangian Eulerian finite element method for path dependent materials, *Computer Methods in Applied Mechanics and Engineering* **58**(2): 227-245.

[15]   Liu W.K., Chang H., Chen J.S., Belytschko T., Zhang Y.F., 1988, Arbitrary Lagrangian–Eulerian Petrov-Galerkin finite elements for nonlinear continua, *Computer Methods in Applied Mechanics and Engineering* **68**(3): 259-310.

[16]   Huerta A., Casadei F., 1994, New ALE application in non-linear fast-transient solid dynamics, *Engineering Computations* **11**(4): 317-345.

[17]   Wang J., Gadala M.S., 1997, Formulation and survey of ALE method in nonlinear solid mechanics, *Finite Elements in Analysis and Design* **24**(4): 253-269.

[18]   Gadala M.S., Wang J., 1998, ALE formulation and its application in solid mechanics, *Computer Methods in Applied Mechanics and Engineering* **167**(1-2): 33-55.

[19]   Gadala M.S., Wang J., 1999, Simulation of metal forming processes with finite element method, *International Journal of Numerical Methods in Engineering* **44**(10): 1397-1428.

[20]   Rodriguez-Ferran A.R., Casadei F., Huerta A., 1998, ALE stress update for transient and quasi-static processes, *International Journal of Numerical Methods in Engineering* **43**: 241-262.

[21]   Aymone J.L.F., Bittencourt E., Creus G.J., 2001, Simulation of 3D metal forming using an arbitrary Lagrangian Eulerian finite element method, *Journal of Materials Processing Technology* **110**(2): 218-232.

[22]   Rodriguez-Ferran A.R., Perez-Foguet A., Huerta A., 2002, Arbitrary Lagrangian–Eulerian (ALE) formulation for hyperelastoplasticity, *International Journal of Numerical Methods in Engineering* **53**(8): 1831-1851.

[23]   Bayoumi H.N., Gadala M.S., 2004, A complete finite element treatment for the fully coupled implicit ALE formulation, *Computational Mechanics* **33**(6): 435-452.

[24]   Khoei A.R., Anahid M., Shahim K., DorMohammadi H., 2008, Arbitrary Lagrangian–Eulerian method in plasticity of pressure-sensitive material: application to powder forming processes, *Computational Mechanics* **42**(1): 13-38.

[25]   Movahhedy M.R., 2000, ALE Simulation of chip formation in orthogonal metal cutting process, PhD dissertation, The University of British Columbia, Canada.

[26]   Gadala M.S., Movahhedy M.R., Wang J., 2002, On the mesh motion for ALE modeling of metal forming processes, *Finite Elements in Analysis and Design* **38**(1): 435-459.

[27]   Ponthot J.P., Belytschko T., 1998 , Arbitrary Lagrangian–Eulerian formulation for element-free Galerkin method, *Computer Methods in Applied Mechanics and Engineering* **152**(1-2): 19-46.

[28]   Gadala M.S., 2004, Recent trends in ALE formulation and its applications in solid mechanics, *Computer Methods in Applied Mechanics and Engineering* **193**: 4247-4275.

[29]   ANSYS Inc., 2009, ANSYS Release 12.1 User's Manual, Mechanical APDL, Swanson Analysis System.

[30]   Belytschko T., Liu W.K., Moran B., 2000, *Nonlinear Finite Elements for Continua and Structures*, John Wiley & Sons, New York.

[31]   Benson D.J., 1989, An efficient, accurate and simple ALE method for nonlinear finite element programs, *Computer Methods in Applied Mechanics and Engineering* **72**(3): 305-350.

[32]   Ponthot J.P., Hogge M., 1991, The use of the Eulerian Lagrangian FEM in metal forming applications including contact and adaptive mesh, in: *Advances in Finite Deformation Problems in Materials Processing and Structures*, ASME Applied Mechanics Division, Atlanta, **125**: 44-64.

[33]   Boman R., Ponthot J.P., 2004, Finite element simulation of lubricated contact in rolling using the arbitrary Lagrangian–Eulerian formulation, *Computer Methods in Applied Mechanics and Engineering* **193**: 4323-4353.

[34]   Martinet F., Chabrand P., 2000, Application of ALE finite element method to a lubricated friction model in sheet metal forming, *International Journal of Solids and Structures* **37**(29): 4005-4031.

[35]   Aymone J.L.F., 2004, Mesh motion techniques for the ALE formulation in 3D large deformation problems, *International Journal of Numerical Methods in Engineering* **59**(14): 1879-1908.

[36]   Miranda I., Ferencz R.M., Hughes T.J.R., 1989, An improved implicit-explicit time integration method for structural dynamics, *Earthquake Engineering and Structural Dynamics* **18**: 643-655.

[37]   Zienkiewicz O.C., Taylor R.L., 2000, The Finite Element Method, vol. 2: Solid Mechanics, McGraw Hill, UK., Fifth Edition.

[38]   Freund L.B., 1998, Dynamic Fracture Mechanics, Cambridge University Press, Berlin.

[39]   Rose L.R.F., 1975, Recent theoretical and experimental results on fast brittle fracture, *International Journal of Fracture* **12**(6): 799-813.

[40]   Rosakis A.J., Duffy J., Freund L.B., 1984, The determination of dynamic fracture toughness of AISI 4340 steel by the shadow spot method, *Journal of the Mechanics and Physics of Solids* **3**(4): 443-460.

[41]   Zehnder A.T., Rosakis A.J., 1990, Dynamic fracture initiation and propagation in 4340-steel under impact loading, *International Journal of Fracture* **43**: 271-285.

[42]   Kalthoff J.F., Beinert J., Winkler S., 1977, Measurement of dynamic stress intensity factors for fast running and arresting cracks in double cantilever beam specimens, in: Fast Fracture and Crack Arrest, edited by G.T. Hahn, M.F. Kanninen, ASTM special technical publication, 161-176.

[43]   Kanninen M.F., Popelar C.H., 1985, *Advanced Fracture Mechanics*, Oxford University Press, New York.

[44]   Yau J., Wang S., Corten H., 1980, A mixed-mode crack analysis of isotropic solids using conservation laws of elasticity, *Journal of Applied Mechanics* **47**: 335-341.

[45]   Nikishkov G.P., Atluri S.N., 1987, Calculation of fracture mechanics parameters for an arbitrary three-dimensional crack, by the 'equivalent domain integral' method, *International Journal for Numerical Methods in Engineering* **24**(9): 1801-1821.

[46]   Shih C., Asaro R., 1988, Elastic-plastic analysis of cracks on bimaterial interfaces: part I-small scale yielding, *Journal of Applied Mechanics* **55**: 299-316.

[47]   Zienkiewicz O.C., Philips D.V., 1971, An automatic mesh generation scheme for plane and curved surfaces by isoparametric coordinates, *International Journal of Numerical Methods in Engineering* **3**(4): 519-528.

[48]   Ravi-Chandar K., Knauss W.G., 1984, An experimental investigation into dynamic fracture. II. Micro structural aspects, *International Journal of Fracture* **26**: 65-80.

[49]   Agrawal, A.K., 2002, Free surface effect on moving crack under impact loading by BEM, *Engineering Analysis with Boundary Elements* **26**: 253-264.